Sparsity Priors for Radiation source Imaging with Collimator-less Position-sensitive Scintillation Detector

Rui Wang[1], Yunhan Yu[1], Qing Ye[1], Ankang Hu[1], Peng Fan[1], Hui Liu[1], Tianpeng Xu[1], Wenzhuo Lu[1], Yaqiang Liu[1], Shi Wang[1], Zhaoxia Wu[1] and Tianyu Ma[1*]
[1]Department of Engineering Physics, Tsinghua University
Beijing, China 100084
maty@tsinghua.edu.cn

***Abstract*— This work aims at imaging gamma radiation sources for security and industrial applications, such as radiation source searching. By using a collimator-less position-sensitive scintillation detector, an angular image of source intensity distribution can be estimated from measuring the photon distribution in the detector by means of image reconstruction. Two types of sparsity priors, the L2-norm of image and the entropy of image are introduced in a MAP reconstruction framework to further improve imaging performance. Monte Carlo simulations and experiments demonstrate the feasibility of the proposed design. MAP reconstruction effectively improves both image resolution and source position estimation accuracy, especially in low count cases. This design is attractive for combined merits of good image resolution, portability and high sensitivity comparing to collimator based gamma cameras when imaging limited number of point sources.**

Keywords—scintillation detector; image reconstruction; prior; image sparisty; radiation source searching; camera

I. INTRODUCTION

RADIOACTIVITY imaging is widely used in security and industrial applications, for instance, it is essential to locate the missing radiation sources in a very fast and accurate way to reduce public and personnel radiation damage. Using traditional counting based devices such as Geiger counter for radiation source searching is time and human power consuming, since such devices are incapable of determining source direction and. Imaging devices such as gamma camera dedicated for medical imaging is capable of positioning the source with high spatial resolution. However, those devices require absorptive collimator to form projection, such as pinhole, parallel-hole or coded-aperture collimators. The collimators are made of heavy metal materials, which thus not only greatly reduces detection sensitivity but also induces considerable carry-on weight. So application of gamma cameras for radiation source searching activities is limited. Compton camera based imaging devices [1, 2] have the capability of 4π imaging and notably improved portability thanks to the absence of collimator. In comparison with collimator based gamma cameras, its resolution is relatively low and it is unsuitable for imaging low-energy gamma sources, when the Compton scattering effect is not prominent.

Researchers [3, 4] have investigated methods that use multiple gamma detectors to determine oriental angle of the radiation sources. By arranging the detectors in a way that each detector attenuates incident photons and causes count decrease of the other detectors, photon count distribution on the detectors is dependent with the source position, and therefore from which the source position can be estimated.

Following this concept, we developed a collimator-less gamma imaging device with position-sensitive scintillation detector arrays. One can imagine that with sufficient number of detector elements, an “image” of angular distribution of source intensity could be generated, similar to the image reconstruction problem in medical imaging.

Considering the Poisson noise nature of photon counts in gamma detector, statistical iterative reconstruction algorithms such as ML-EM are naturally proper choice for image reconstruction. In this work, we evaluate the feasibility of using a 2D position sensitive LYSO+SiPM detector that was previously developed for PET imaging to implement a gamma source imager. Both simulation and experimental studies were conducted.

Unlike medical imaging, a gamma source image is usually sparse in space, as the sources can be treated as point-type when the source-to-detector distance is much larger than the detector size and thus far-field assumption is applicable. Besides, in radiation source searching activities, the number of sources to be found is most likely limited. Therefore, this work focuses on exploring a way to exploit the image domain sparsity in gamma source imaging scenarios to improve image resolution and sensitivity. Two types of regularization functions are evaluated: 1) Maximizing a L2-norm prior that favors sparsity in the image domain; 2) Minimizing an entropy prior that encourages sparsity in the image gray-level domain. 3D Monte Carlo simulation and preliminary experimental studies were conducted to test the efficacy of the above priors at different count levels.

DOI: 10.12059/Fully3D.2017-11-3203007

II. MATERIALS AND METHODS

A. Problem Formation

Figure 1 shows a conceptual drawing of the proposed approach. A position sensitive gamma detector is placed in the radiation field. When the distance between a gamma source and the detector is much larger than the detector size, the radiation source can be considered as a parallel-beam source, and its position can be represented by the oriental angles. When the detector is illuminated by the gamma source, the photon count distribution over the detector is dependent on both source orientation and photon attenuation inside the detector. Let image $x_i(\theta_i,\varphi_i)$ represent the source intensity at direction bin (θ_i,φ_i), projection p_j be the count in j-th detector element, the projection formation process can be written as:

$$p_j = \sum_i a_{i,j} x_i(\theta_i,\varphi_i) + noise \quad (1)$$

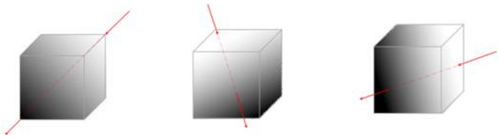

Figure 1. Concept diagram of the radioactive- source imaging with a position sensitive detector. The red line represents the direction from which a gamma source is illuminating the detector, and the gray colors in the detector represents detector count.

Where the system matrix $\{a_{i,j}\}$ stands for the probability that a photon coming from direction (θ_i,φ_i) is detected in j-th detector. Assuming that the detector is made of uniform material with linear attenuation coefficient μ , As shown in Figure 2, $\{a_{i,j}\}$ can be calculated by:

$$a_{i,j} = \int (e^{-\mu l_{j,1}} - e^{-\mu l_{j,2}})\, \mathrm{d}S \ , \quad (2)$$

Where $\mathrm{d}S$ is the integral element across the front surface of j-th detector element.

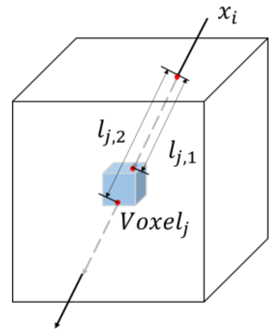

Figure 2. Diagram of the image formation process. The probability that a photon coming from angle x_i is detected in voxel j is dependent on $l_{j,1}$, $l_{j,2}$ and the attenuation coefficient of the crystal.

Therefore, the task of radiation source searching is interpreted as to reconstruct $x_i(\theta_i,\varphi_i)$ from p_j.

B. Image Reconstruction

Considering the Poisson noise nature of measured projection, the log-likelihood cost function is defined as:

$$L(X)_{ML} = \log\left\{\prod_j \frac{\left(\sum_i a_{ij}x_j\right)^{p_j}}{p_j!} e^{-\left(\sum_i a_{ij}x_j\right)}\right\}. \quad (3)$$

The corresponding ML-EM update equation is:

$$x_i^{k+1} = \frac{x_i^k}{\sum_j a_{ij}} \sum_j \frac{a_{ij}p_j}{\sum_{i'} a_{i'j}x_{i'}^k}. \quad (4)$$

To encourage image sparsity, a L2-norm image prior is included in the cost function:

$$L(X)_{MAP} = \log\left\{\prod_j \frac{\left(\sum_i a_{ij}x_j\right)^{p_j}}{p_j!} e^{-\left(\sum_i a_{ij}x_j\right)}\right\} + \beta\|X\|_2, \quad (5)$$

The corresponding one-step-late (OSL) update equation is

$$x_i^{k+1} = \frac{x_i^k}{\sum_j a_{ij} - \beta\frac{x_i^k}{\|X\|_2}} \sum_j \frac{a_{ij}p_j}{\sum_i a_{ij}x_i^k}. \quad (6)$$

The image entropy form cost function is defined as:

$$L(X)_{MAP} = \log\left\{\prod_j \frac{\left(\sum_i a_{ij}x_j\right)^{p_j}}{p_j!} e^{-\left(\sum_i a_{ij}x_j\right)}\right\} - \beta H(X) \quad (7)$$

$$H(X) = \int -p(x)\log p(x) . \quad (8)$$

In which, $p(x)$ stands for the probability density of reconstructed image.

The corresponding OSL update equation is

$$x_i^{k+1} = \frac{x_i^k}{\sum_j a_{ij} + \beta \frac{\partial H(x^k)}{\partial x_i}} \sum_j \frac{a_{ij} p_j}{\sum_i a_{ij} x_i^k} . \quad (9)$$

Details of the discrete approximation of $H(X)$ and its gradient can be found in [5].

.

C. Monte Carlo Simulation

A 16 x 16 x 16 LYSO crystal array was simulated. The crystal size was 2 x 2 x 2 mm^3. Ideal intrinsic spatial resolution was assumed, and the energy resolution was 10% at 511 keV. A 0.3-mCi point source were placed at certain oriental angular positions with 1-meter distance to the center of detector. ~ 4 M counts were acquired for each source position. Lu^{176} background activity was not simulated.

Two sets of data with lower counts, 30k and 0.8k were also extracted to evaluate imaging performance at low count case. The projection data at (60°,30e) and (150°,120°), and the projection data at (60°,30°), (150°,120°) and (30°,210°) were also summed to mimic a 2-point-source and a 3-point-source detector situation.

ML-EM, MAP-EM with maximum L2-norm prior (MAP -L2 in short), and MAP-EM with minimum Entropy (MAP -Ep in short) algorithms were implemented for image reconstruction. in 3D case, a 360 x 180-pixel image (1 deg bin size) were reconstructed from the 16 x16 x16 projection. β values for MAP-L2 and MAP-Ep were empirically chosen at each count level for best image performance.

D. Experiment

In experiment, a LYSO + SiPM detector was used. The detector has 16 x 16 LYSO crystals with 2 x 2 x 7 mm^3 size. 8 x 8 Sensl FJ30035 SiPM array was coupled to the crystal array. Readout and data acquisition electronics were developed in our own lab.

A F^{18}-FDG point source was used in experiment. The activity was 0.15 mCi at the start of measurement. The point source was manually placed at 8 angular positions (approximately 0°, 30°, 45°, 60°, 90°, and 180°). At each position, 2 M counts were acquired in ~120 s. A relatively narrow energy window, 511keV ± 10%, was applied to reduce the impact of Compton scattering photons. Background activity from Lu^{176} was measured for 2 hours which was used for background subtraction.

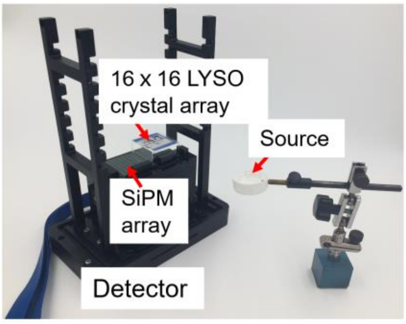

Figure 3 Experimental setup. The LYSO+SiPM detector was placed in a fixture. The source was manually placed at different angular positions surrounding the detector.

In both simulation and experiment, the system matrices were derived from Monte Carlo simulated data of a spherical surface source surrounding the detector. $\{a_{i,j}\}$ was calculated by dividing counts in j-th detector bin that come from i-th image bin and source activity in i-th image bin.

III. RESULTS

A. Simulation – single point source at high count level

Figure 4 and Figure 5 shows representative reconstructed images of one point source (θ= 90°, φ =60°) with MLEM after 200, 500, and 1000 iterations. Images at other angular positions show similar shape.

Figure 6 shows that as the value of β increases, the FWHM decreases. If the value of β is appropriate, the image can be converged to a single point immediately. MAP_Ep algorithm shows the similar law. Therefore, we can reduce the FWHM by using MAP algorithm with an appropriate value of β.

Figure 7 shows the Reconstructed images with three different algorithms for the point source (θ= 90°, φ =60°) along the φ direction . As shown in Figure 7, the MLEM image has broader distribution for a point source (θ= 60°) compared with MAP_L2 and MAP_Ep images. MAP-Ep and MAP-L2 images with uniform initials converged to a point centered at 57° and 58° respectively. In comparison, if taking the MLEM update results after 500 iterations as the initial image, 500 following iterations of both MAP-Ep and MAP-L2 presented single-point image with accurate angular estimation. Similar results were achieved when the source is at other angular positions other than 0°, where all the algorithms tests offers perfect angular estimation results. Therefore, in what follows, images with 500 MLEM iteration were taken as initial values for all MAP reconstructions.

Table 1 and Table 2 summarizes imaging performance for single point source at (45°,0°), (75°,0°), (90°,30°), (90°,60°) with 3 different reconstruction approaches. 1000 MLEM iterations, 500 MLEM iterations + 500 MAP_L2 iterations, and 500 MLEM iterations + 500 MAP_Ep iterations were performed respectively. All the images reconstructed with MAP-L2 and MAP_Ep converged to a single point. In all the cases tested, the absolute direction estimation error, which is between the centroid of the reconstruction image and the source position, is less than 1°.

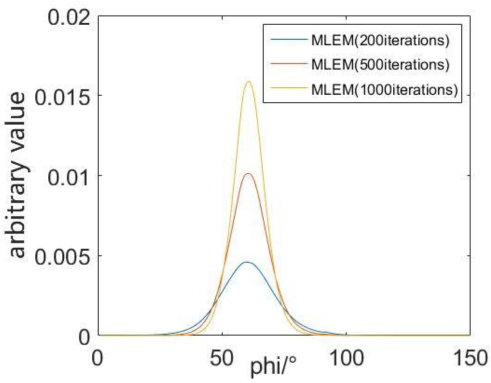

Figure 4 ML-EM Reconstructed images with 200, 500 and 1000 iterations along φ direction for point source θ= 90⁰ , φ=60°.

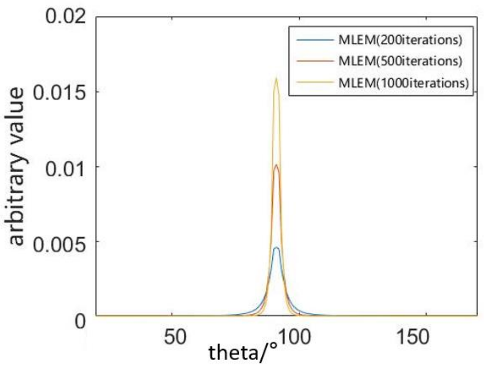

Figure 5 ML-EM Reconstructed images with 200, 500 and 1000 iterations along θ direction for point source θ= 90⁰ , φ=60°.

Table 1 ESTIMATION ACCURACY FOR POINT SOURCE AT DIFFERENT POSITIONS ALONG THE ϑ DIRECTION

Simulation angle (ϑ,φ) /°	**Absolute direction estimation error in the ϑ direction/°**		
	ML-EM	**MAP_L2 with MLEM initial**	**MAP_Ep with MLEM initial**
(45,0)	1	1	1
(75,0)	1	1	1
(90,30)	0	0	0
(90,60)	0	0	0

Table 2 ESTIMATION ACCURACY FOR POINT SOURCE AT DIFFERENT POSITIONS ALONG THE φ DIRECTION

Simulation angle (ϑ,φ) /°	**Absolute direction estimation error in the φ direction/°**		
	ML-EM	**MAP_L2 with MLEM initial**	**MAP_Ep with MLEM initial**
(45,0)	1	1	1
(75,0)	0	0	0
(90,30)	0	0	0
(90,60)	0	0	0

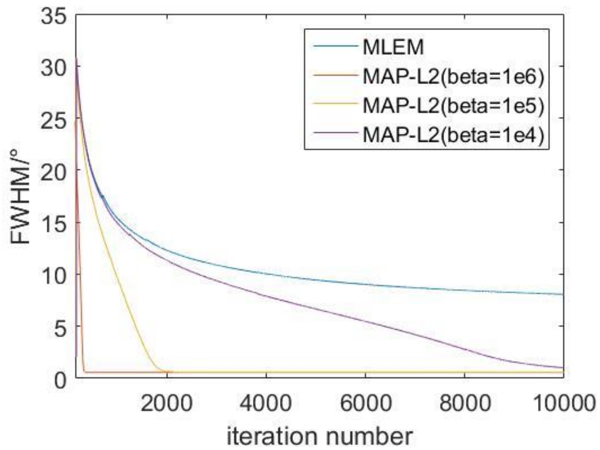

Figure 6 FWHM with MLEM and MAP-L2 algorithms for the point source θ = 90^0 , φ=60° along φ direction. MAP-L2 algorithms are with different β values.

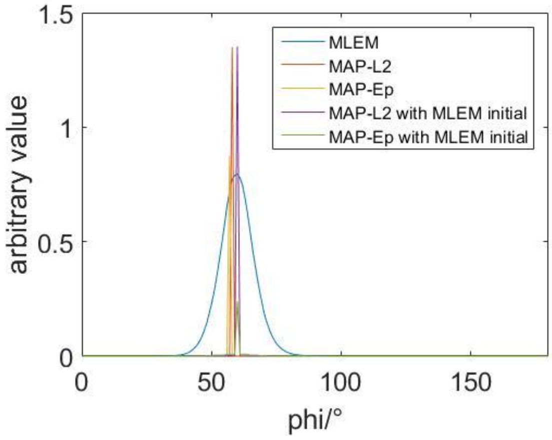

Figure 7 Reconstructed images with different reconstruction algorithms for the point source θ = 90^0 , φ=60° along φ direction. Aside from MLEM, MAP-Ep, MAP_L2 results (1000 iterations) whose iteration are started from a uniform image, MAP_EP and MAP_L2 reconstruction images (after 500 iterations) that use an initial image with 500 MLEM iterations are also shown. MAP_Ep and MAP_L2 images are almost identical and overlap with each other.

B. Simulation – single point source at low count level

Table 3 shows reconstructed images of a point source at(90°, 60°) with different reconstruction algorithms at three count levels (~0.8k counts, ~30k counts , and ~4M counts). We ran the iterations to converge in all cases. In all cases tested, MLEM did not converge to a single point, and both MAP algorithms converged to a single point. However, the estimated position was slightly worse with 0.8k counts – The source was placed at 55° by MAP_L2 and 55° by MAP_Ep along the φ direction. However, we can still get the accurate position along the θ position with 0.8k counts.

Table 3 ABSOLUTE ESTIMATION ACCURACY FOR POINT SOURCE AT DIFFERENT POSITIONS

Angle (90°,60°)	**counts**	**Absolute direction estimation error /°**		
		ML-EM	**MAP_L2 with MLEM initial**	**MAP_Ep with MLEM initial**
***ϑ* (90°)**	**4M**	0	0	0
	30k	0	0	0
	0.8k	1	1	1
***φ* (60°)**	**4M**	0	0	0
	30k	0	0	0
	0.8k	5	5	5

C. Simulation – multiple point sources

Figure 5 presents two reconstructed images with multiple point sources with simulation data with 1000 MLEM iterations. For both the two point sources and the three sources cases, MLEM reconstructed sources at correct positions.

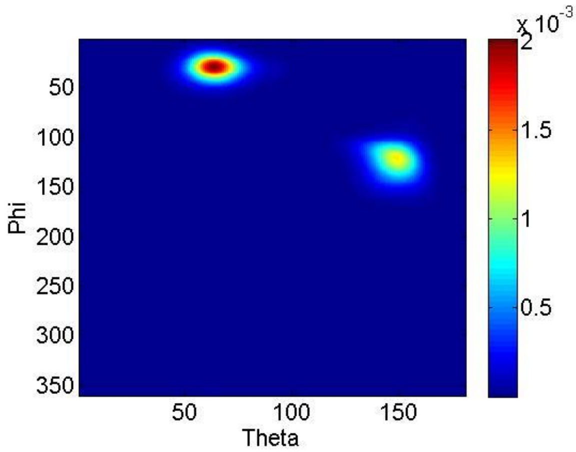

(a)

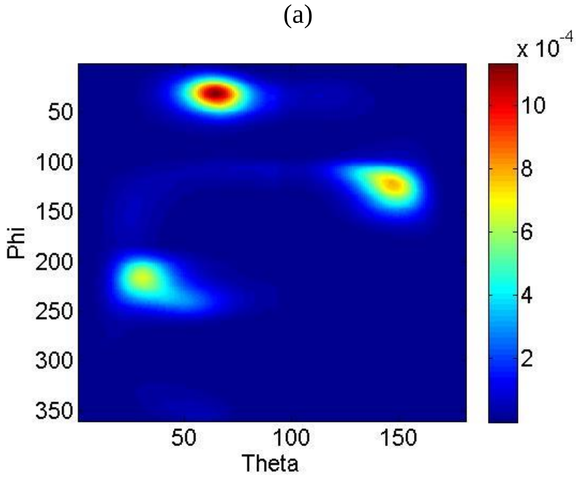

(b)

Figure 5 reconstructed images for: (a) two point sources at (60°, 30°) and (150°,120°) with 4M counts; and (b) three point sources at (60°, 30°), (150°,120°) and (30°,210°) with 4M counts, with three reconstruction algorithms.

D. Experimental results

Similar to the findings in simulation studies, at a relative high count level, all the algorithms yields reasonable images for a single point source. MAP reconstructions achieves better resolution than MLEM. Shown in Figure 6 is one representative case with a point source located at ~45° .

Table 4 summarizes point source position estimation accuracy studies for experimental data. As the source was manually placed at each acquisition and the absolute position is not precisely unknown, the calculated centroids from 2M-count projection are listed in 1st, 4th and 7th columns as the reference values. These values between different algorithms are quite close. At low count level, 10 groups of statistically independent noisy projections were extracted out of the complete list-mode dataset, the centroids were calculated from the reconstructed images, and the average of the absolute value of the difference between these centroid and that from 2M count image was calculated for each case, and are listed in the rest of columns. One can see that from 200 count projections, the source position estimation error introduced by noise is less than 5° in average. MAP algorithms gives slightly better results than MLEM.

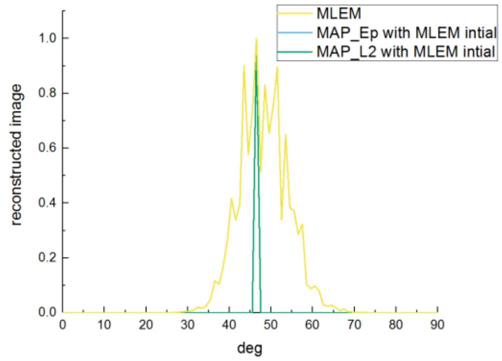

(c)

Figure 6 Reconstructed images of a single point source in experiment. 1000 MLEM iterations, or 700 MAP iterations following 300 MLEM iterations were performed. MAP_Ep and MAP_L2 images overlap with each other.

Table 4 RELATIVE ESTIMATION ERROR FOR POINT SOURCE AT DIFFERENT POSITIONS: EXPERIMENTAL RESULTS

Average direction estimation accuracy/°								
MLEM			**MAP_L2 with MLEM initial**			**MAP_Ep with MLEM initial**		
2M (reference)	**200**	**20**	**2M (reference)**	**200**	**20**	**2M (reference)**	**200**	**20**
0	4.1	7.6	0	2.8	6.1	0	2.8	6.1
19	7.4	9.9	19	7.4	10.4	19	7.4	10.4
37	6.9	34.2	37	5.9	35.8	37	5.7	35.8
47	4.5	10.3	47	4.5	10.3	47	4.5	10.3
68	4.4	16.8	68	6.1	16.8	68	6.1	16.8
83	2.2	3.5	85	1.9	3.9	85	1.9	3.9
90	5.4	4.8	90	3.4	4.6	90	3.4	4.6
180	1.8	20.8	180	1.7	20.8	180	1.7	20.8
average	4.58	13.48		4.21	13.59		4.19	13.59

IV. CONCLUSION

In this work, we present a novel imaging based approach to locate and monitor gamma sources for industrial and safety applications. Image reconstruction methods are discussed, and two priors that favor image domain sparsity are evaluated. Simulation and experimental studies consistently demonstrate the feasibility of the proposed system design. MAP reconstruction effectively improves both image resolution and source position estimation accuracy, especially in low count cases. This design is attractive for combined merits of good image resolution, portability and high sensitivity comparing to mechanical collimator based gamma cameras when imaging limited number of point sources.

REFERENCES

[1] C. E. Lehner, H. Zhong, and Z. Feng, "4π Compton imaging using a 3-D position-sensitive CdZnTe detector via weighted list-mode maximum likelihood," *IEEE Transactions on Nuclear Science,* vol. 51, no. 4, pp. 1618-1624, 2004.

[2] D. Xu and Z. He, "Filtered Back-Projection in 4 pi Compton Imaging With a Single 3D Position Sensitive CdZnTe Detector," *IEEE Transactions on Nuclear Science,* vol. 53, no. 5, pp. 2787-2796, 2006.

[3] C. L. Larsson and S. Djeffal, "Development of a directional gamma ray probe," in *IEEE Nuclear Science Symposium Conference Record, 2005*, 2005, vol. 1, pp. 16-18.

[4] Y. Shirakawa, "Development of a direction finding gamma-ray detector," *Nuclear Instruments and Methods in Physics Research Section B: Beam Interactions with Materials and Atoms,* vol. 263, no. 1, pp. 58-62, 10// 2007.

[5] Y. Yu, S. Yao, W. Shi, Y. Liu, and T. Ma, "PET-MR Joint Reconstruction with Information Theoretic Priors," presented at the IEEE Nuclear Science Symposium and Medical Imaging Conference, Strausbrag, France, 2016.